

Effect of oxidation on intrinsic residual stress in amorphous silicon carbide films

Felix Deku¹,^{ORCID} Shakil Mohammed,² Alexandra Joshi-Imre,¹ Jimin Maeng,¹ Vindhya Danda,¹ Timothy J. Gardner,³ Stuart F. Cogan¹

¹Department of Bioengineering, University of Texas at Dallas, Richardson, Texas

²Department of Materials Science and Engineering, University of Texas at Dallas, Richardson, Texas

³Department of Biology and Department of Biomedical Engineering, Boston University, Boston, Massachusetts

Received 5 June 2018; revised 26 August 2018; accepted 16 September 2018

Published online 00 Month 2018 in Wiley Online Library (wileyonlinelibrary.com). DOI: 10.1002/jbm.b.34258

Abstract: The change in residual stress in plasma enhanced chemical vapor deposition amorphous silicon carbide (a-SiC:H) films exposed to air and wet ambient environments is investigated. A close relationship between stress change and deposition condition is identified from mechanical and chemical characterization of a-SiC:H films. Evidence of amorphous silicon carbide films reacting with oxygen and water vapor in the ambient environment are presented. The effect of deposition parameters on oxidation and stress variation in a-SiC:H film is studied. It is found that the films deposited at low temperature or power are susceptible to oxidation and undergo a

notable increase in compressive stress over time. Furthermore, the films deposited at sufficiently high temperature (≥ 325 C) and power density (≥ 0.2 W cm⁻²) do not exhibit pronounced oxidation or temporal stress variation. These results serve as the basis for developing amorphous silicon carbide based dielectric encapsulation for implantable medical devices. © 2018 Wiley Periodicals, Inc. *J Biomed Mater Res B Part B*: 00B: 000–000, 2018.

Key Words: amorphous silicon carbide, residual stress, a-SiC oxidation, air stability, PECVD

How to cite this article: Deku F, Mohammed S, Joshi-Imre A, Maeng J, Danda V, Gardner TJ, Cogan SF. 2018. Effect of oxidation on intrinsic residual stress in amorphous silicon carbide films. *J Biomed Mater Res B Part B*. 2018;9999:9999:1–8.

INTRODUCTION

Thin-film coatings of amorphous silicon carbide (a-SiC), have been used as a protective coating for implantable neural devices,^{1–6} orthopedic implants⁷ and coronary stents.^{8–10} The a-SiC is usually deposited by plasma enhanced chemical vapor deposition (PECVD), which allows for moderately low-temperature deposition (≤ 400 °C), high deposition rates and precise control of residual film stress. Residual stress may be intrinsic, arising from hydrogen incorporated in the film during deposition, or extrinsic, due to differential thermal expansion between the a-SiC film and the coated substrate. Although most studies have associated residual stress of PECVD a-SiC (a-SiC:H) films to deposition conditions, we are interested in the stress evolution post-deposition in response to the ambient environment as changes in the residual stress state can alter the planarity of implantable thin-film devices fabricated from a-SiC:H films.⁵ Loss of planarity may prevent devices from being inserted into tissue or, if residual stresses change after implantation, there is the possibility of tissue damage or unpredictable changes in device performance.

The intrinsic stress in a-SiC:H is usually compressive arising from the incorporation of hydrogen as evident from

the Si–H peak intensities in Fourier transform infrared (FTIR) spectra and the monotonic relationship between film stress and the peak intensity.^{11,12} Hydrogen incorporation occurs because of incomplete decomposition of the hydrogen-containing precursors. These weakly bonded hydrogen atoms permit the carbide surface to oxidize to a few nanometers when exposed to ambient air.¹³ The reaction kinetics are faster in films with high carbon and hydrogen compositions¹⁴ and films with higher micro-void densities.¹⁵ Previous published research on controlling residual stress has identified power density, temperature, gas ratio, pressure as well as He or Ar dilution of the reactive gas as factors influencing the residual stress in a-SiC:H films.^{16–21}

In the present study, the time-dependent change of residual stress in a-SiC:H films is investigated. The relationship between film oxidation and stress change, along with the effects of different deposition conditions is examined. X-ray photoelectron spectroscopy (XPS) and FTIR spectroscopy were used to understand the molecular origin of stress variation over time in these films. Evidence of a-SiC:H films reacting with water vapor and oxygen (O₂) from ambient environments is presented. This study is intended to inform

Correspondence: F. Deku; e-mail: felix.deku@utdallas.edu

Contract grant sponsor: National Institutes of Health; contract grant number: U01 NS090454

the selection of deposition conditions to produce low-stress and air stable a-SiC:H dielectric coatings for chronic implantable medical devices.

MATERIALS AND METHODS

Amorphous silicon carbide film deposition

A PlasmaTherm Unaxis 790 series PECVD system with a platen area of $\sim 1000 \text{ cm}^2$ was used to deposit the a-SiC:H films. The films were deposited on 100 mm Si (100) prime wafers (University Wafer) along with double-sided polished (DSP) high resistivity Si wafers (Silicon Valley Microelectronics, Santa Clara, California) for FTIR measurements. Three sets of films were deposited for the study with the deposition condition ranges selected based on earlier studies.^{1,11,12} The first set was deposited at different temperatures, from 150°C to 350°C at a fixed power density of 0.27 W cm^{-2} . The second set was deposited at different power densities, ranging from 0.05 to 0.32 W cm^{-2} , at a fixed temperature of 350°C. The chamber was maintained at a pressure of 1000 mTorr with the total gas flow fixed at 800 sccm using Ar as the carrier gas. For all depositions, a $\text{SiH}_4:\text{CH}_4$ gas flow rate ratio of 1:3 was used. The thickness of the films was maintained close to $1 \mu\text{m}$ by varying deposition time. The a-SiC:H films were exposed to air at room temperature, and the intrinsic stress in these films was monitored once every 7 days over a period of 28 days.

The third set of films were deposited at 150°C and 350°C, and a power density of 0.27 W cm^{-2} , and were exposed to various environments including dry air (7 ppm of H_2O , $\sim 20\%$ O_2), deionized (DI) water, nitrogen (N_2 ; 99.998%), and O_2 (99.994%). Changes in intrinsic stress in these films was monitored for 24 h.

Amorphous silicon carbide film characterization

A Nanometric NanoSpec 6100 analyzer (Nano metrics, Milpitas, California) was used to measure the average film thickness from 20 different points randomly across the wafer. A Toho Technology FLX-2320-S system was used to measure the film stress. The stress values were estimated from changes in the radius of curvature of the silicon substrate due to the deposition of the a-SiC:H film using the Stoney equation²² and have an accuracy of $<2.5\%$ of the measured stress for values above 40 MPa based on manufacturer's specifications. FTIR transmittance spectra were recorded using a ThermoElectron Nicolet iS50 spectrometer (Thermo Scientific, Waltham, Massachusetts) with a deuterated triglycine sulfate detector at a wavelength resolution of 4 cm^{-1} . A PHI VersaProbe II spectrometer (Physical Electronics, Chanhassen, Minnesota) equipped with an Al K_α monochromated X-ray source ($h\nu = 1486.7 \text{ eV}$) was used to collect the XPS data. The films were pre-sputtered with 1 keV Ar ions for 10 min to remove a thin layer of the a-SiC:H surface prior to spectral collection. Voigt line shapes in conjunction with a Shirley background subtraction utilizing "AAnalyzer" software was used to fit the spectra.²³

RESULTS

Residual stress stability

The residual stress of air-exposed a-SiC:H films was monitored over a period of 28 days. The time-evolution of the residual stress as a function of deposition temperature and power density is shown in Figure 1. Figure 1(a) shows the residual stress in films deposited at temperatures ranging from 150°C to 350°C at a constant power density of 0.27 W cm^{-2} . The residual stress in the as-deposited films (at day 0) becomes less compressive as deposition temperature is increased (-230 MPa for $T_D = 150^\circ\text{C}$ to -100 MPa for $T_D = 350^\circ\text{C}$), similar to results reported elsewhere.²¹ The stress in the films deposited at 325°C and 350°C remained approximately unchanged over time. However, in the lower-temperature films ($T_D = 250^\circ\text{C}$ and $T_D = 150^\circ\text{C}$), a large increase in compressive stress was observed. Between the initial measurement (day 0) and the first measurement at

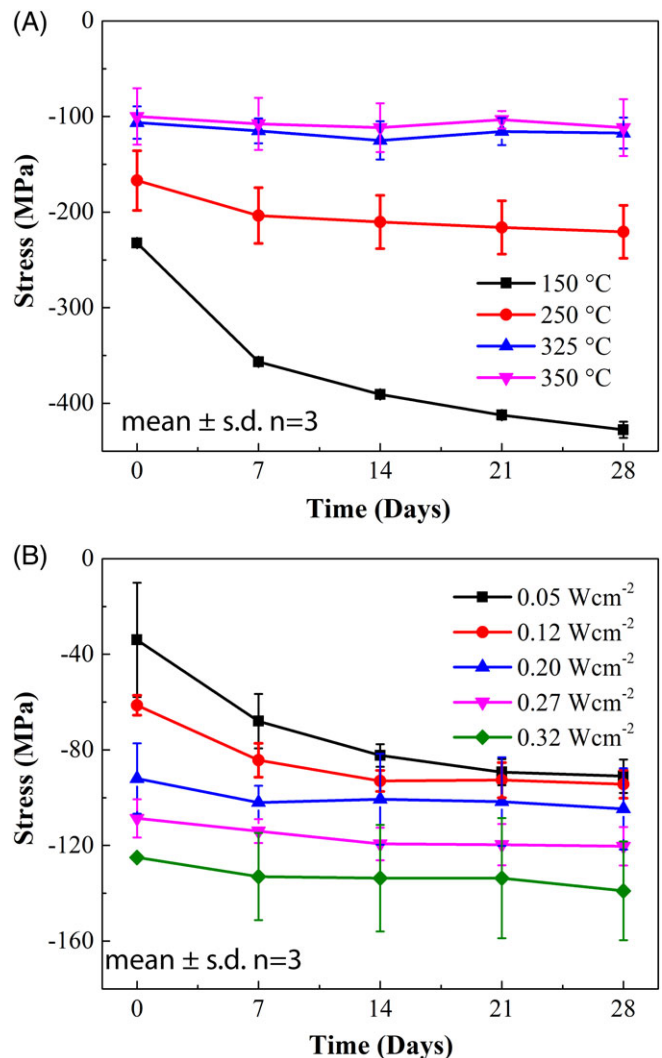


FIGURE 1. Residual stress in air-exposed a-SiC:H films deposited at (a) various deposition temperatures and power density of 0.27 W cm^{-2} and (b) various power densities at a deposition temperature of 350°C, monitored over a period of 28 days. Data are reported as mean \pm 1 SD, $n = 3$.

day 7, the magnitude of the compressive stress increased from -163 to -203 MPa (24.5% increase), and from -226 to -356 MPa (57.5% increase), for $T_D = 250^\circ\text{C}$ and $T_D = 150^\circ\text{C}$, respectively. The stress became increasingly compressive as the air-exposure period was extended to 28 days. Figure 1(b) shows the stress variation in films deposited at power densities ranging from 0.05 to 0.32 W cm^{-2} with the platen temperature controlled to 350°C .

The compressive stress of as-deposited films increases with increasing deposition power (-35 MPa for 0.05 W cm^{-2} to -125 MPa for 0.32 W cm^{-2}), similar to previous published studies.²¹ The present work demonstrates that the power density at which the films are deposited also influences the changes in film stress over time. The residual stress remains relatively unchanged in the films deposited at power density equal to or greater than 0.2 W cm^{-2} , while more pronounced changes are observed at low-power deposition conditions.

XPS and FTIR analysis

XPS spectra collected 28 days post-deposition are plotted in Figure 2. The Si $2p$, C $1s$ and O $1s$ regions were charge compensated by shifting the data to center the O $1s$ peak at 532.2 eV prior to fitting the spectra. The Si $2p$ region [Figure 2(a)] was fitted using doublet peaks considering the spin-orbit splitting of the orbital, but only the convolution of the doublet is displayed for clarity. The doublet peak represented by Si $2p_{3/2}$ and Si $2p_{1/2}$ are separated only by 0.6 eV and have an intensity ratio of 2:1.²⁴

The overall Si $2p$ peak position was observed at lower binding energies for higher deposition temperatures. For films deposited at $T_D = 350^\circ\text{C}$ and 325°C , a single peak centered at $\sim 100.2\text{ eV}$, typical of the Si-C bond,²⁵ was observed. Two distinct fitted peaks were observed for films deposited at 150°C and 250°C . The primary peak appears at 100.8 eV in the 250°C film and at 101 eV in the 150°C film. These peaks were assigned to the Si-O-C bond, as the peak position has previously been associated with SiOC_3 ²⁶ or $\text{Si}_2\text{OC}_{2.2}$ ²⁷ bonding. The secondary peak at 102.1 eV can be assigned to either O-rich SiO_3 ²⁸ or a sub-stoichiometric SiO_x phase.²⁹

The C $1s$ spectra, shown in Figure 2(b), exhibits two peaks for each film. The peak at 283.3 eV in both 350°C and 325°C films is due to C-Si bonding. The C-Si peak shifts to higher energies at lower deposition temperatures, which is attributed to the presence of C-Si-O bonding structures. The shift of the C-Si peak in the C $1s$ region corresponds to the observed shift of Si-C peaks at lower deposition temperatures in the Si $2p$ region. The peak at 284.7 eV is due to C-C bonding and does not shift with deposition temperature but appears to increase in intensity relative to the C-Si-O bonding as the deposition temperature is decreased.

The O $1s$ region of both the 350°C and the 325°C deposited films show very low peak intensities, as shown in Figure 2(c). The intensity of O $1s$ increases in the 250°C films and further increases in the 150°C films. Two peaks were identified for the low temperature films, with the

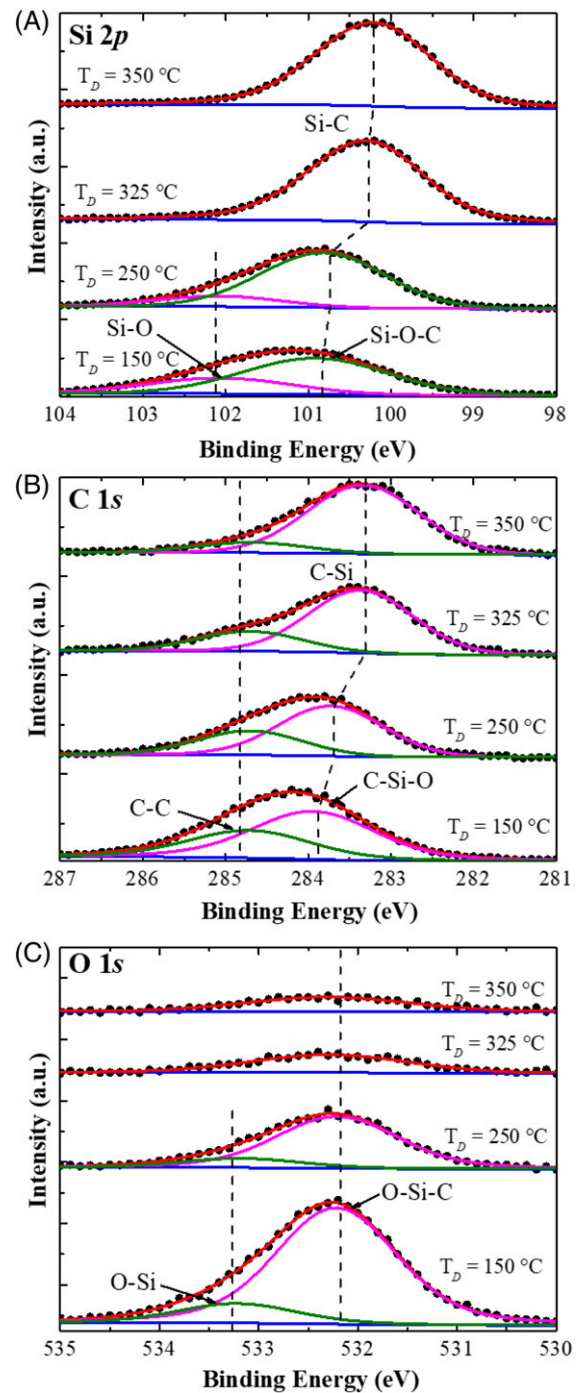


FIGURE 2. The effect of deposition temperature on the XPS spectra of a-SiC:H air-exposed for 28 days. The dashed lines represent the peak positions of (a) Si $2p$, (b) C $1s$, and (c) O $1s$. a-SiC:H, amorphous silicon carbide; XPS, X-ray photoelectron spectroscopy.

primary peak located at 532.2 eV arising from O-Si-C bonding, and the secondary peak at 533.2 eV arising from O-Si bonding. The O-Si peaks in the O $1s$ region corresponds with the Si-O peaks in the Si $2p$ region for the low-temperature deposited films.

The film composition x , defined as the ratio of the number of silicon atoms to the total number of silicon and carbon atoms, $x = \text{Si}/(\text{Si} + \text{C})$ was estimated using the atomic

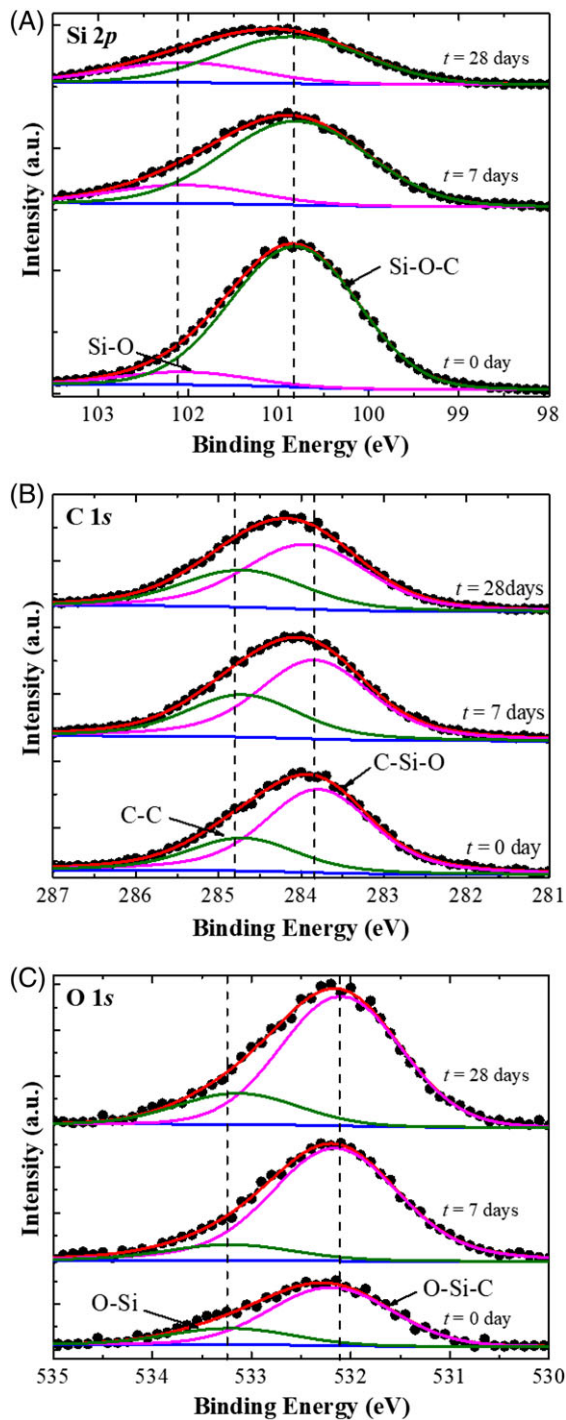


FIGURE 3. XPS of a-SiC:H deposited at $T_D = 150^\circ\text{C}$ and characterized after 0, 7, and 28 days of air exposure. The dashed lines represent the peak positions of (a) Si 2p, (b) C 1s, and (c) O 1s. a-SiC:H, amorphous silicon carbide; XPS, X-ray photoelectron spectroscopy.

concentration calculated from the XPS spectra. The nominal composition was approximately $x = 0.5$, with a trend toward increasing Si concentration as the deposition temperature was increased.

XPS spectra showing the compositional changes in the film deposited at $T_D = 150^\circ\text{C}$, at time points 0 (as-deposited), 7 and 28 days post deposition are shown in Figure 3. The

peak intensity of the O-Si bonding in the O 1s region and Si-O bonding in the Si 2p regions increased over time. Also, the O-Si-C peak intensity in the O 1s region increased and the Si-O-C peak intensity in the Si 2p region decreased as time progressed. The peak positions of the Si 2p and the C 1s did not change relative to O 1s over the observed period.

Figure 4 shows the IR transmittance spectra of the silicon carbide films that were deposited on high-resistivity (3–5 k Ω -cm) DSP silicon wafers. The changes in the spectra were monitored immediately after deposition and then 1, 2, 7, and 28 days post-deposition. The peaks observed conform to those published in the literature.^{30–34} The peak at 607 cm^{-1} is due to the Si-Si phonon absorption from the substrate.¹

The most intense peak at 780 cm^{-1} has been reported to be the Si-C stretching mode, and the shoulder at ~ 1020 cm^{-1} has been identified as either a Si-CH₂ or a Si-O-Si stretching, or both.^{30–32} The peak at ~ 2100 cm^{-1} arises from the Si-H stretching, and various C-H_n stretching modes appear at ~ 2900 cm^{-1} .^{11,35} Figure 4(a–c) shows spectra collected for all deposition temperature (T_D) films after deposition (day 0), day 7 and day 28 respectively, while Figure 4(d) shows an overlay of the FTIR spectra for films with a $T_D = 150^\circ\text{C}$ as time progressed. For the as-deposited a-SiC:H films, the peak intensities for the Si-C bond were almost the same regardless of the deposition temperature, while the Si-O-Si, Si-CH₃ and Si-H peaks increased with decreasing temperature. Also, the Si-H peak shifts to higher frequency as the deposition temperature decreases. The peak intensities and peak positions did not change for films deposited at higher temperatures ($T_D = 350^\circ\text{C}$ and $T_D = 325^\circ\text{C}$) on exposure to air. The films deposited at lower temperature (especially at $T_D = 150^\circ\text{C}$) exhibit a gradual decrease of the Si-H peak intensity at ~ 2100 cm^{-1} , with a peak shift to higher frequencies (inset), and a noticeable increase of the Si-O-Si peak intensities at the ~ 1020 cm^{-1} shoulder as shown in Figure 4(d).

Examination of Figure 4(d) also reveals the growth of a broad band at ~ 3425 cm^{-1} which has been previously assigned to the hydroxyl (O-H) group.^{36,37} A plot of the Si-H peak position as a function of time for the $T_D = 150^\circ\text{C}$ film is shown in Figure 5, including a Gaussian fit (inset) suggesting that this absorption band arises primarily from Si-H vibration with a small contribution from Si-H₂.^{38,39}

Furthermore, the area under the Si-O-Si and Si-C absorption band was integrated and shown in Figure 6 as a function of air exposure time for the $T_D = 150^\circ\text{C}$ film. The Si-C bonding remains constant, whereas the Si-O-Si bonding is observed to increase over time.

Effect of environment on stress change

To evaluate the relative effects of different environmental conditions on a-SiC:H films stress, a short-term study was conducted in which a set of films deposited at $T_D = 150^\circ\text{C}$ and 350°C were monitored over a 24-h period under exposure to laboratory air, dry air (7 ppm of H₂O), N₂, O₂, and DI water. As shown in Figure 7, residual stress of the films deposited at $T_D = 350^\circ\text{C}$ remained nearly unchanged over

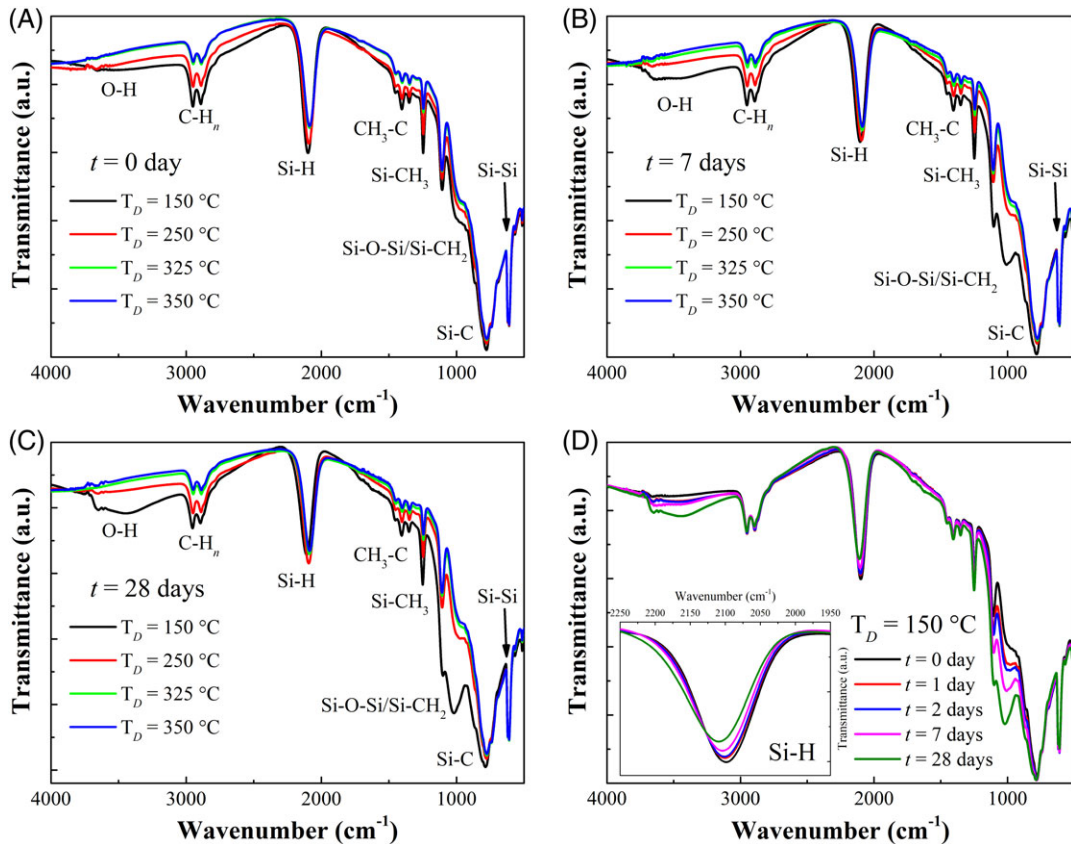


FIGURE 4. Representative FTIR spectra of air-exposed a-SiC:H films deposited at various temperatures are recorded (a) after deposition, (b) 7 days post-deposition, and (c) 28 days post-deposition. The evolution in the FTIR spectra for the a-SiC:H deposited at $T_D = 150^\circ\text{C}$ over the 28-day post-deposition period are compared directly in (d). The inset in (d) shows the shift and change in intensity of the Si-H stretching band. a-SiC:H, amorphous silicon carbide; FTIR, Fourier transform infrared.

24 h of exposure, while films deposited at $T_D = 150^\circ\text{C}$ changed to varying degrees depending on the environment. For all a-SiC:H films except those stored under N_2 , a trend of increasing compressive stress is observed. The films stored under dry air and O_2 showed an increase of 17% and 25%, respectively. The film stored under DI water and air showed the highest increase in the compressive stress, as high as 32%, during the 24-h study period.

DISCUSSION

As expected, the results presented show that residual stresses in as-deposited a-SiC:H films are strongly dependent on both deposition temperature and power. The results also show that the stress in a-SiC:H films deposited at low temperature ($T_D = 150^\circ\text{C}$) changes over time to an extent that is determined by the degree of exposure to O_2 or water. Films deposited at low temperature or low power density ($T_D \leq 250^\circ\text{C}$ or $<0.2 \text{ W cm}^{-2}$ power density), as shown in Figure 1, increase in compressive stress on air exposure. Since the films for studying the effect of deposition temperature were all deposited at a high-power density of 0.27 W cm^{-2} , and the films for investigating the effect of power density were all deposited at 350°C , the results indicate proper selection of both parameters is necessary for

making a-SiC:H films with stable stress. Low-temperature films exhibit oxidation over time as observed from the XPS data in Figure 2. Since the XPS data were collected after 10 min of Ar-sputtering to remove surface layers, the data represent sub-surface bonding in the a-SiC:H. Similarly, the XPS data in Figure 2 show Si-O and O-Si peaks at Si 2p and O 1s regions indicating sub-surface oxidation in the low temperature deposited films. The peak intensities increase with time of air exposure (Figure 3).

From changes in FTIR and XPS spectra, oxidation of air-exposed low-temperature a-SiC:H films is ongoing over at least a 28-day period, and the oxidation corresponds to an increase in compressive residual film stress. The $T_D = 150^\circ\text{C}$ films also show an increase in Si-O-Si bonding and a decrease in Si-H bonding [inset of Figure 4(d)], suggesting that Si-H, from incomplete reaction of the SiH_4 precursor, is being oxidized to Si-O. Since the C-C and C-Si-O peak intensities are unaffected with time [Figure 3(b)], oxidation does not appear to involve carbon. Since the FTIR transmission spectra in Figure 4, show notable intensity changes in the Si-O-Si and the O-H vibration modes at 1020 and 3425 cm^{-1} , respectively, it seems likely that the oxidation is occurring in the bulk of the film as well as at the surface of the $T_D = 150^\circ\text{C}$ films. While XPS in Figure 2 shows that the sub-surface of the low temperature films is predominantly

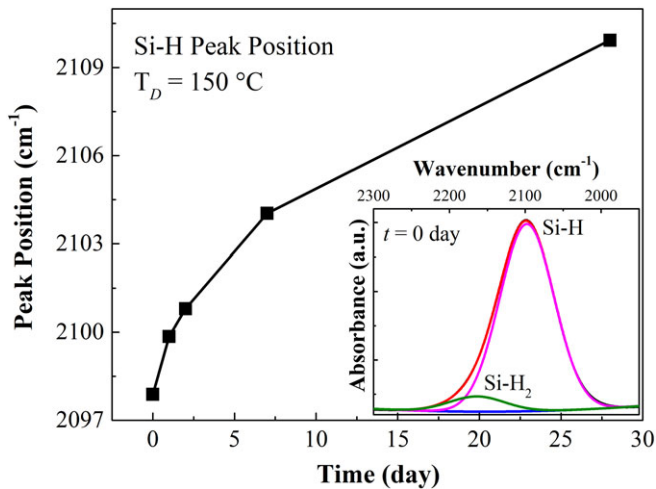


FIGURE 5. The FTIR shift in the Si-H peak for the film deposited at $T_D = 150^\circ\text{C}$ is shown in the plot. (Inset) The de-convoluted peaks show Si-H and Si-H₂ stretching modes. FTIR, Fourier transform infrared.

composed of silicon-oxy-carbide at initial time points, FTIR reveals a strong Si-C peak (the highest intensity peak) whose band intensity remains relatively constant over time and is not affected by the growing peak at its shoulder representing the increasing Si-O-Si content (Figure 6). This result further suggests that the Si-C bonding in the $T_D = 150^\circ\text{C}$ is stable to air exposure, and the observed oxidation is predominately related to the high Si-H content of the low temperature films.

From Figure 7, residual stress in the low-temperature deposited films does not vary greatly when exposed to a N₂ environment, suggesting that the residual stresses in a-SiC:H films will remain nearly unchanged in the absence of O₂ or water. In the presence of O₂, as evident from the film stored in dry air (~20% O₂) and O₂ ambient (100% O₂), the rapid

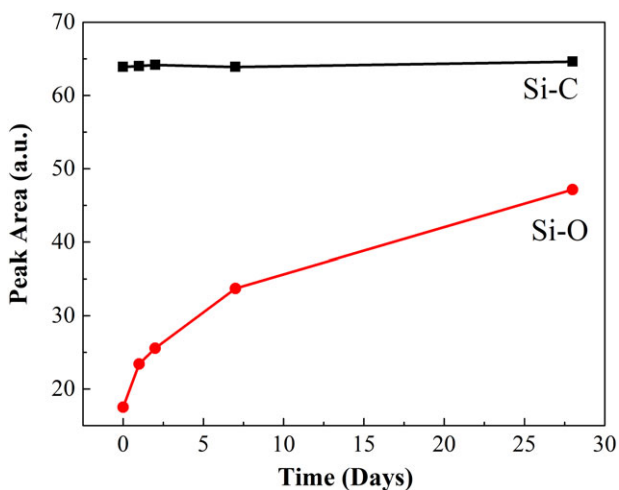


FIGURE 6. Area of the Si-C, and Si-O infrared absorption bands for $T_D = 150^\circ\text{C}$ a-SiC:H as a function of air exposure time. The intensity of the Si-C band remains unchanged, while the Si-O band increased in intensity with time corresponding to observed changes in the O 1s XPS data in Figure 3c. a-SiC:H, amorphous silicon carbide; XPS, X-ray photoelectron spectroscopy.

oxidation of the film results in a rapid increase in compressive stress; at a rate dependent on O₂ concentration. A pronounced increase in compressive stress is also observed on air exposure, but less in dry air (Figure 7) implicating water vapor as well as O₂ gas in the oxidation of the low deposition temperature a-SiC:H. Finally, the largest oxidative effect and subsequent increase in compressive stress is observed for films soaked in deionized water. From these results, it is evident that both O₂ and water react with a-SiC:H to increase compressive film stresses. Similarly, reaction with O₂ and water vapor have also been shown to produce compressive stresses in other thin films such as aluminum⁴⁰ and silicon monoxide.⁴¹ The environmental conditions investigated in this work reflect the O₂, water vapor exposure, and liquid water the a-SiC:H films may encounter during thin-film processing and device fabrication. Residual stress changes in deionized water also suggest that stress changes may be driven by exposure to the physiological environment.

The increase in compressive stress in the low-temperature or low-power a-SiC:H films is therefore attributed to the oxidation of Si-H and the incorporation of larger O₂ or hydroxyl moieties into the a-SiC:H film. A consequence of the change in residual stress of the a-SiC:H is the loss of stress balance in thin-film structures. The lower density a-SiC:H may also not be as effective an encapsulation layer as the higher density films.

Our primary focus is the development of devices for chronic intracortical stimulation and recording. These multi-layer devices include both insulating and conductive thin films,^{4,5} and will require careful balancing of film stress and film thickness to preserve a planar geometry.⁵ Any deviation from planarity will likely exacerbate tissue damage and hemorrhage during insertion into target neural tissues or cause the device to deviate from its intended insertion path. Changes in a-SiC film stress after implantation may also be a concern since a stress change is expected to progressively induce curvature in the device resulting in potentially harmful tissue displacement. Recently, devices that actuate in vivo

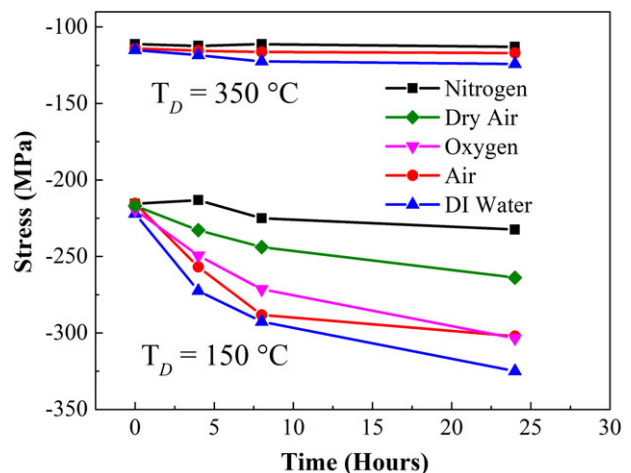


FIGURE 7. Residual stress in a-SiC:H films deposited at $T_D = 150^\circ\text{C}$ under exposure to various ambient environments over a period of 24 h. a-SiC:H, amorphous silicon carbide.

to produce a localized displacement of cortical recording electrodes have been investigated with the objective of optimizing the neuron-electrode interface.⁴² Localized changes in residual stress may be one approach to inducing small localized displacements in implanted devices.

This study focused on the effects of deposition conditions on the magnitude and stability of residual stresses in a-SiC:H thin films. Films deposited under conditions that produced a stable residual stress were always observed to be under compression with a typical as-deposited stress of -80 to -120 MPa (Figure 1). This magnitude of residual stress is enough to induce curvature in a-SiC:H films, requiring a stress balancing strategy.⁵ Of interest for future work would be the development of deposition conditions that lead to a-SiC:H films with a more neutral residual stress that is also stable. In addition, the investigation of the effect of reactive oxygen species and other potentially damaging chemical constituents associated with the foreign body response to implanted devices should also be investigated.⁴³

CONCLUSIONS

The change in residual stress in PECVD a-SiC:H films exposed to air and wet ambient environments was investigated, and a relationship between film oxidation and stress changes identified. The increase in compressive residual stress is associated with oxidation of Si-H which is more prevalent in the films deposited at low temperature or at low power. To achieve stable low-stress a-SiC:H films, it is desirable to deposit these films at high temperature ($\geq 325^\circ\text{C}$) and power density ($\geq 0.2 \text{ W cm}^{-2}$). These findings should serve as a guide for developing a-SiC:H based dielectric coatings for implantable medical devices where thin-film stress management and long-term stability are essential. While these results and earlier work¹ suggest an optimum deposition temperature of $>300^\circ\text{C}$ for PECVD a-SiC:H, alternative approaches to densifying PECVD films including the use of very high frequency generators, multiple frequencies or pulsed plasma deposition could be investigated as a means of obtaining stable, low stress films at lower deposition temperatures.

ACKNOWLEDGMENTS

The authors wish to thank the University of Texas at Dallas Natural Sciences and Engineering Research Laboratory cleanroom staff, especially Dr. Gordon Pollack and Mr. Scott R. Riekena, for their support in maintenance of the PECVD tool. We also want to thank Rebecca Frederick for assisting with the preparation of this manuscript. This work was conducted under NIH grant U01NS090454 awarded to Dr. Timothy J. Gardner of Boston University.

AUTHOR CONTRIBUTIONS

FD and SFC conceived and conceptualized the study. FD and VD prepared the a-SiC:H films and performed stress measurements. FD and SM performed the FTIR and XPS measurements. SM performed the analysis of the FTIR and XPS measurements. FD, SM, AJ, JM, TJG, and SFC provided useful discussions, interpreted results and contributed to manuscript preparation.

CONFLICT OF INTEREST

None declared.

REFERENCES

- Cogan SF, Edell DJ, Guzelian A a, Ping Liu Y, Edell R. Plasma-enhanced chemical vapor deposited silicon carbide as an implantable dielectric coating. *J Biomed Mater Res A* 2003;67:856–867. <https://doi.org/10.1002/jbm.a.10152>.
- Hsu JM, Tathireddy P, Rieth L, Normann AR, Solzbacher F. Characterization of a-SiC_x:H thin films as an encapsulation material for integrated silicon based neural interface devices. *Thin Solid Films* 2007;516:34–41. <https://doi.org/10.1016/j.tsf.2007.04.050>.
- Knaack GL, McHail DG, Borda G, Koo BS, Peixoto N, Cogan SF, Dumas TC, Pancrazio JJ. In vivo characterization of amorphous silicon carbide as a biomaterial for chronic neural interfaces. *Front Neurosci* 2016;10:301. <https://doi.org/10.3389/FNINS.2016.00301>.
- Lei X, Kane S, Cogan S, Lorach H, Galambos L, Huie P, Mathieson K, Kamins T, Harris J, Palanker D. SiC protective coating for photovoltaic retinal prosthesis. *J Neural Eng* 2016;13:046016. <https://doi.org/10.1088/1741-2560/13/4/046016>.
- Deku F, Cohen Y, Joshi-Imre A, Kanneganti A, Gardner TJ, Cogan SF. Amorphous silicon carbide ultramicroelectrode arrays for neural stimulation and recording. *J Neural Eng* 2018;15:016007. <https://doi.org/10.1088/1741-2552/aa8f8b>.
- Diaz-Botia CA, Luna LE, Neely RM, Chamanzar M, Carraro C, Carmena JM, Sabes PN, Maboudian R, Maharbiz MM. A silicon carbide array for electrocorticography and peripheral nerve recording. *J Neural Eng* 2017;14:056006. <https://doi.org/10.1088/1741-2552/aa7698>.
- Sella C, Lecoœur J, Sampeur Y, Catania P. Corrosion resistance of amorphous hydrogenated SiC and diamond-like coatings deposited by r.f.-plasma-enhanced chemical vapour deposition. *Surf Coatings Technol* 1993;60:577–583. [https://doi.org/10.1016/0257-8972\(93\)90156-1](https://doi.org/10.1016/0257-8972(93)90156-1).
- Kalnins U, Erglis A, Dinne I, Kumsars I, Jegere S. Clinical outcomes of silicon carbide coated stents in patients with coronary artery disease. *Med Sci Monit* 2002;8:PI16–20. <http://www.ncbi.nlm.nih.gov/pubmed/11859292>.
- Hamm CW, Hugenholtz PG. Silicon carbide-coated stents in patients with acute coronary syndrome. *Catheter Cardiovasc Interv* 2003;60:375–381. <https://doi.org/10.1002/ccd.10656>.
- Amon M, Bolz A, Schaldach M. Improvement of stenting therapy with a silicon carbide coated tantalum stent. *J Mater Sci Mater Med* 1996;7:273–278. <https://doi.org/10.1007/BF00058566>.
- Jean A, Chaker M, Diawara Y, Leung PK, Gat E, Mercier PP, Pépin H, Gujrathi S, Ross GG, Kieffer JC. Characterization of a-SiC:H films produced in a standard plasma enhanced chemical vapor deposition system for X-ray mask application. *J Appl Phys* 1992;72:3110–3115. <https://doi.org/10.1063/1.351471>.
- Windischmann H. Intrinsic stress and mechanical properties of hydrogenated silicon carbide produced by plasma-enhanced chemical vapor deposition. *J Vac Sci Technol A Vacuum, Surfaces, Film* 1991;9:2459–2463. <https://doi.org/10.1116/1.577256>.
- Lee W-Y. X-ray photoelectron spectroscopy and auger electron spectroscopy studies of glow discharge Si_{1-x}C_x:H films. *J Appl Phys* 1980;51:3365–3372. <https://doi.org/10.1063/1.328049>.
- Eldridge JM, Moore JO, Olive G, Dunton V. Oxidation of plasma-deposited $\alpha\text{-Si}[\text{sub } x]\text{C}[\text{sub } 1-x]\text{H}$ films. *J Electrochem Soc* 1990;137:2266. <https://doi.org/10.1149/1.2086925>.
- Mastelaro V, Flank AM, Fantini MCA, Bittencourt DRS, Carreño MNP, Pereyra I. On the structural properties of a-Si_{1-x}C_x:H thin films. *J Appl Phys* 1996;79:1324–1329. <https://doi.org/10.1063/1.361029>.
- M. Avram, A. Avram, A. Bragaru, Bangtao Chen, D.P. Poenar, C. Iliescu, Low stress PECVD amorphous silicon carbide for MEMS applications, in: CAS 2010 Proceedings (International Semiconductor Conference, IEEE, 2010: pp. 239–242. doi:<https://doi.org/10.1109/SMICND.2010.5650647>.
- Oliveira AR, Carreño MNP. Post thermal annealing crystallization and reactive ion etching of SiC films produced by PECVD. *J Non Cryst Solids* 2006;352:1392–1397. <https://doi.org/10.1016/j.jnoncrsol.2006.01.075>.

18. Iliescu C, Chen B, Poenar DP, Lee YY. PECVD amorphous silicon carbide membranes for cell culturing. *Sens Actuators B* 2008;129: 404–411. <https://doi.org/10.1016/j.snb.2007.08.043>.
19. Sarro PM, Deboer CR, Korkmaz E, Laros JMW. Low-stress PECVD SiC thin films for IC-compatible microstructures. *Sensors Actuators, A Phys* 1998;67:175–180. [https://doi.org/10.1016/S0924-4247\(97\)01730-5](https://doi.org/10.1016/S0924-4247(97)01730-5).
20. Wu D-S, Horng R-H, Chan C-C, Lee Y-S. Plasma-deposited amorphous silicon carbide films for micromachined fluidic channels. *Appl Surf Sci* 1999;144–145:708–712. [https://doi.org/10.1016/S0169-4332\(98\)00911-8](https://doi.org/10.1016/S0169-4332(98)00911-8).
21. Iliescu C, Avram M, Chen B, Popescu A, Dumitrescu V, Poenar DP, Sterian A, Vrtacnik D, Amon S, Sterian P. Residual stress in thin films PECVD depositions: a review. *J Optoelectron Adv Mater* 2011; 13:387–394.
22. Stoney GG. The tension of metallic films deposited by electrolysis. *Proc R Soc A Math Phys Eng Sci* 1909;82:172–175. <https://doi.org/10.1098/rspa.1909.0021>.
23. Shirley DA. High-resolution x-ray photoemission spectrum of the valence bands of gold. *Phys Rev B* 1972;5:4709–4714. <https://doi.org/10.1103/PhysRevB.5.4709>.
24. Ohishi K, Hattori T. Periodic changes in SiO₂/Si(111) interface structures with Progress of thermal oxidation. *Jpn J Appl Phys* 1994;33: L675–L678. <https://doi.org/10.1143/JJAP.33.L675>.
25. Smith KL, Black KM. Characterization of the treated surfaces of silicon alloyed pyrolytic carbon and SiC. *J Vac Sci Technol A Vacuum, Surfaces, Film* 1984;2:744–747. <https://doi.org/10.1116/1.572562>.
26. Powers JM, Somorjai GA. The surface oxidation of alpha-silicon carbide by O₂ from 300 to 1373 K. *Surf Sci* 1991;244:39–50. [https://doi.org/10.1016/0039-6028\(91\)90167-Q](https://doi.org/10.1016/0039-6028(91)90167-Q).
27. Schelz S, Oelhafen P. Interface properties of hydrogenated amorphous carbon films on SiO₂ and SiO_{1.2}: an in situ photoelectron study. *Surf Sci Lett* 1992;279:A105. [https://doi.org/10.1016/0167-2584\(92\)90214-P](https://doi.org/10.1016/0167-2584(92)90214-P).
28. Önneby C, Pantano CG. Silicon oxycarbide formation on SiC surfaces and at the SiC/SiO₂ interface. *J Vac Sci Technol A Vacuum, Surfaces, Film* 1997;15:1597–1602. <https://doi.org/10.1116/1.580951>.
29. Lee RC, Aita CR, Tran NC. The air-exposed surface of sputter deposited silicon carbide studied by X-ray photoelectron spectroscopy. *J Vac Sci Technol A Vacuum, Surfaces, Film* 1991;9:1351–1354. <https://doi.org/10.1116/1.577625>.
30. Fonseca JLC, Apperley DC, Badyal JPS. Plasma polymerization of tetramethylsilane. *Chem Mater* 1993;5:1676–1682. <https://doi.org/10.1021/cm00035a015>.
31. Demichelis F, Crovini G, Pirri CF, Tresso E. Infrared vibrational spectra of hydrogenated amorphous and microcrystalline silicon-carbon alloys. *Philos Mag Part B* 1993;68:329–340. <https://doi.org/10.1080/13642819308215290>.
32. Fujimoto F, Ootuka A, Komaki K, Iwata Y, Yamane I, Yamashita H, Hashimoto Y, Tawada Y, Nishimura K, Okamoto H, Hamakawa Y. Hydrogen content in a-SiC:H films prepared by plasma decomposition of Silane and methane or ethylene. *Jpn J Appl Phys* 1984;23: 810–814. <https://doi.org/10.1143/JJAP.23.810>.
33. Huran J, Hrubcin L, Kobzev APA, Liday J. Properties of amorphous silicon carbide films prepared by PECVD. *Vacuum* 1996;47: 1223–1225. [https://doi.org/10.1016/0042-207X\(96\)00128-5](https://doi.org/10.1016/0042-207X(96)00128-5).
34. McCurdy PR, Truitt JM, Fisher ER. Pulsed and continuous wave plasma deposition of amorphous, hydrogenated silicon carbide from SiH₄/CH₄ plasmas. *J Vac Sci Technol A Vacuum, Surfaces, Film* 1999;17:2475–2484. <https://doi.org/10.1116/1.582105>.
35. Wang Y, Lin J, Huan CH. Multiphase structure of hydrogenated amorphous silicon carbide thin films. *Mater Sci Eng B* 2002;95: 43–50. [https://doi.org/10.1016/S0921-5107\(02\)00204-0](https://doi.org/10.1016/S0921-5107(02)00204-0).
36. Singh AK, Pantano CG. Surface chemistry and structure of silicon oxycarbide gels and glasses. *J Sol-Gel Sci Technol* 8 (1997) 371–376. [doi:https://doi.org/10.1023/A:1026467908933](https://doi.org/10.1023/A:1026467908933).
37. Wang Y, He MY, Chen RY. Fabrication of mechanically robust anti-reflective films using silica nanoparticles with enhanced surface hydroxyl groups. *J Mater Chem A* 2015;3:1609–1618. <https://doi.org/10.1039/C4TA04840G>.
38. Wieder H, Cardona M, Guarnieri CR. Vibrational spectrum of hydrogenated amorphous Si-C films. *Phys Status Solidi* 1979;92:99–112. <https://doi.org/10.1002/pssb.2220920112>.
39. Tawada Y, Tsuge K, Kondo M, Okamoto H, Hamakawa Y. Properties and structure of a-SiC:H for high-efficiency a-Si solar cell. *J Appl Phys* 1982;53:5273–5281. <https://doi.org/10.1063/1.331363>.
40. D'Heurle FM. Aluminum films deposited by rf sputtering. *Metall Mater Trans B* 1970;1:725–732. <https://doi.org/10.1007/BF02811600>.
41. Priest J, Caswell HL, Budo Y. Mechanical stresses in silicon oxide films. *Vacuum* 1962;12:301–306. [https://doi.org/10.1016/0042-207X\(62\)90182-3](https://doi.org/10.1016/0042-207X(62)90182-3).
42. Xie C, Liu J, Fu TM, Dai X, Zhou W, Lieber CM. Three-dimensional macroporous nanoelectronic networks as minimally invasive brain probes. *Nat Mater* 2015;14:1286–1292. <https://doi.org/10.1038/nmat4427>.
43. Takmakov PA. Electrochemistry of a robust neural Interface. *Electrochem Soc Interface* 2017;26:49–51. <https://doi.org/10.1149/2.F05173if>.